Spin scan tomographic imager

H. Hovland*
Norwegian Defence Research Establishment, P. O. Box 25, N-2027 Kjeller, Norway

ABSTRACT

A novel imaging device based on tomographic reconstruction is presented. The imager is based on rotating an image of the scene onto a linear detector array, and then reconstructing a 2-dimensional image from the detector array signal using tomographic reconstruction techniques. Similar in many ways to the conical scan tomographic scanning (TOSCA) imager, the spin scan TOSCA imager features several improvements compared to its predecessors, mainly because the linear array covers the whole scene and hence in principle can collect 100% of the incoming photons. In addition to presenting the theory behind the device and its sensitivity to noise, non-uniformity and errors, an experimental uncooled mid-wave infrared imager demonstrator is also presented, together with images of test targets, both the final result as well as the incremental steps in the imaging reconstruction process.

Keywords: Tomography, tomographic image processing, imaging systems, infrared imaging, image reconstruction techniques, Fourier optics and signal processing.

1. INTRODUCTION

Tomographic scanning (TOSCA) imaging have been refined from the realization that a classical conical scan reticle tracker could have imaging properties[1] to more dedicated designs, where a moving circular aperture would remove aliasing[2] and the large sector based reticle was replaced by a thin slit reticle to significantly improve both the signal-to-noise ratio and the dynamic range[3]. These improvements lead to the realizations of the first practical imagers based on this scheme[4-5], operating in both the visible and the infrared band, including multispectral operation. The principle and schematics of the first experimental conical scan TOSCA imager is presented in Figure 1. Here, a circular aperture limits the field of view, and a set of thin slits are scanned across an image of the scene at regularly distributed angles. The light transmitted through both the circular aperture and thin slits are collected by a detector, the whole assembly thus acting as multiplexed line scanners (each slit produces one line scan). After the set of line scans are recorded, a reconstruction using tomographic reconstruction techniques can be applied to the data[6].

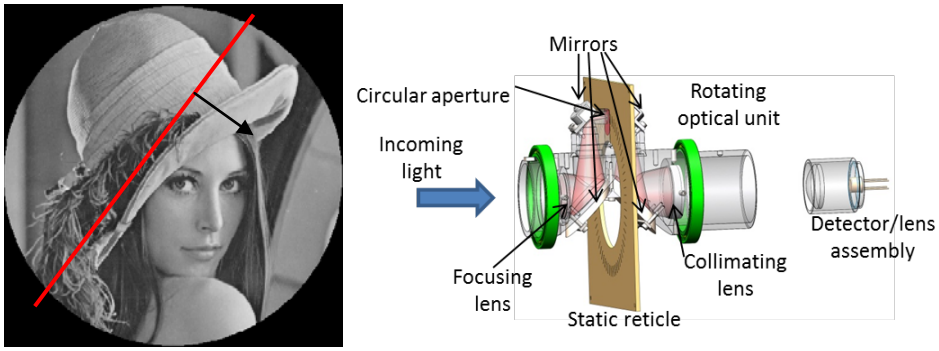

Figure 1. Left: Principle of the TOSCA imager. A scene is limited by a circular aperture (indicated in black) and then scanned by a second, thin slit aperture (red, moving according to the black arrow). The light passing through the apertures is collected by a single detector. This scan is repeated at regularly distributed angles. Right: Schematics of the first experimental conical scan TOSCA imager[4]. Incoming light is focused onto a static reticle via a focusing lens and a rotating pair of mirrors that move the light sideways, and a circular moving reticle that limits the field of view. The image thus retains a fixed orientation, enabling the thin slits on the static reticle to scan the scene image at regularly distributed angles. Behind the static reticle, another pair of rotating mirrors moves the light back along the rotational center to enable collection of the light from a fixed detector.

*harald.hovland@ffi.no; phone (+47) 63 80 73 12; fax (+47) 63 80 72 12; www.ffi.no

In a paper thoroughly describing the theory behind the TOSCA concept[7], it was pointed out that replacing the reticle and the single detector with a circular array of stripe detectors (each followed by individual amplifier stages) could enhance the sensor. In fact, to avoid aliasing with the reticle configuration, each line scan must be finished before the next scan can begin. Using a circular detector array means the detector does not have this requirement, meaning several scans can overlap. The consequences are the following:

- The line detectors can be located closer to each other, enabling a smaller scan circle, leading to smaller overall sensor dimensions.
- The smaller scan circle also enables the use of optics with lower f/#, enabling a smaller spot size. The smaller spot size again enables narrower detector widths and an even smaller scan circle.
- A smaller scan circle also enables slower scan speeds across the detectors for a given frame rate, reducing required bandwidth and associated noise.
- Multiple detectors in the field of view simultaneously increase detector coverage of the field of view, increasing overall sensor sensitivity

The potential performance is significantly improved in terms of sensitivity. As an example, the improvement is roughly 2 orders of magnitude for a layout using 65 detectors.

This concept, however promising, was not pursued, as a newer, even more promising concept has been conceived: The spin scan TOSCA imager, first presented in 2014[8].

2. SPIN SCAN TOSCA IMAGER

In the spin scan TOSCA imager, an image of the scene is projected onto, while being rotated relative to a linear array of parallel narrow detector lines. A circular aperture can be placed in front of the linear array (which will typically have a square active area) to obtain a circular field of view that remains unchanged during rotation. The schematics of the spin scan TOSCA imager is shown in Figure 2. The spin scan TOSCA imager features several improvements compared to the conical scan array-based TOSCA imager:

- A compact monolithic detector structure. Using parallel detectors enables economical use of detector space without having to cut out individual detectors and reorient them. (Cutting and reorienting potentially also causes signal degradation due to alignment issues).
- The whole field of view can be covered by detectors, enabling all photons could in principle be captured. This enhances the overall efficiency by a factor of roughly 4, compared to the conical scan array-based concept. In addition, it also means any rapid transient process could also be monitored, and be localized at least in one dimension.
- The higher detector density also reduces the detector bandwidth requirement, further reducing noise levels.

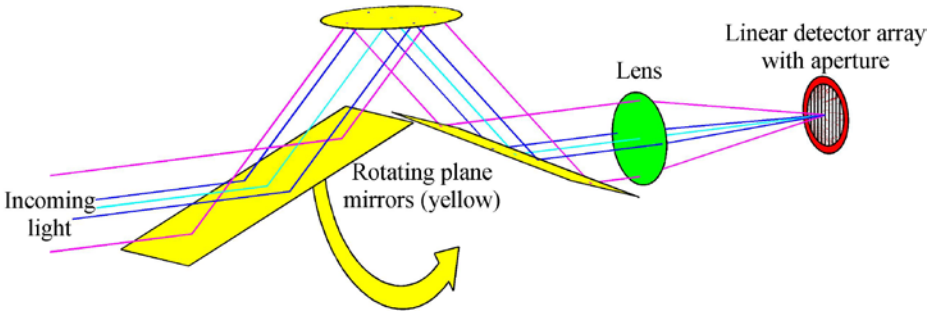

Figure 2. Spin scan TOSCA imager principle. The image of the scene is projected onto a linear detector array while rotating with respect to the array. A circular aperture maintains a circular field of view, acting as a field stop. In this configuration three plane mirrors acts as the rotating scan mechanism, followed by a lens to focus incoming light. Image from Hovland[8].

Although the scan system is different from the conical scan TOSCA imager, once the recordings are made, the signal processing of the set of line scans are processed in the same way.

The scan mechanism presented in Figure 2 is simple to conceive and use, and enables a high level of freedom with regards to the choice of focusing optics and wavelength range, but is relatively bulky. In order for the rotation of the scene image with respect to the scene, it is necessary to either rotate the scene, rotate the linear array, or use rotating optics that flips the scene. Rotating the scene limits itself to controlled scenes of limited size. The rotation of the linear array is easy if it is mounted on a forward-looking and rotating projectile or other body, but is in principle also possible if the rotating sensor holds electronics such as preamplifiers and analog to digital conversion circuitry. Much easier, though, is the use of rotating optics which flips the image. One way to achieve this this is through the use of an odd number of mirrors, either using three mirrors as depicted in Figure 2, or through the use of a Dove prism, where one mirror is used. An alternative, compact device was presented by Hovland[8], consisting of a toroidal primary mirror followed by a toroidal or cylindrical secondary mirror. A less compact, but equivalent setup using refractive optics (for example using two cylindrical lenses and a regular lens with rotational symmetry) were also proposed in the same paper.

In the current work a new and very compact solution is proposed, not yet found elsewhere in the literature by the author. The optical element is shown in Figure 3. It consists of a compound of a cylindrical lens focusing in one orientation, and a 1-dimensional Fresnel reflector in the other orientation. The particularity of this Fresnel reflector is that its focal plane is behind it. Similar Fresnel reflectors have been extensively used in X-ray optics. Two orthogonal one-dimensional Fresnel reflectors have been proposed in the Schmidt optics[9]. A 2-dimensional version of a similar reflector is found in nature in the lobster's eye, and was first proposed for use in X-ray optics by Angel[10].

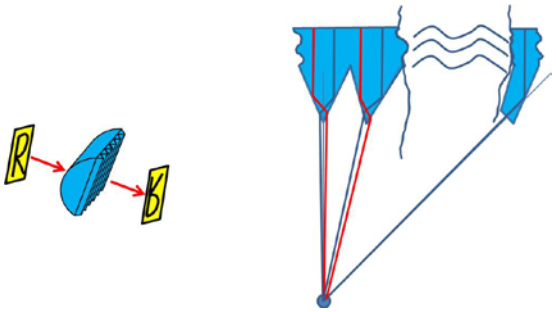

Figure 3. Left: New compound element consisting of a cylinder lens followed by a kind of Fresnel reflector letting light pass. This setup enables flipping the image. Right: Details of the Fresnel reflectors, both at and near the optical axis, and further out on the side. The incoming beam (from the top) is first refracted by the cylinder lens (not illustrated), then reflected by total internal reflection, and then refracted towards a common focal point. Not seen in the image, the lower end surfaces are actually curved to enable a beam spot smaller than the Fresnel zone itself.

What is peculiar with the Fresnel mirror part is that the focal point of the element moves in the opposite direction with the incoming light, compared to a regular convex lens. Having a regular cylinder lens acting in one direction and the Fresnel mirror acting in the other direction enables flipping the image of the scene. This again enables rotating the (flipped) image of the scene when the optics rotates around the optical axis of the incoming light.

The mirrors could in principle be made out of metal sheets or metal coated substrates, but with a sufficiently high refractive index, total internal reflection surfaces could be used to create a highly efficient Fresnel reflector. Using this approach, it is possible to incorporate both the cylinder lens and the orthogonally oriented Fresnel reflector in a single compound element. Assuming the second (exit) surface is normal to the light beam leaving the element after it has been reflected, for an f-number of 1.0, it is sufficient to have a refractive index above 2.6. This index could even be lowered by adjusting the orientation of the surface through which the light exits.

The Fresnel reflector does not work at normal incidence, however, two opposing total internal reflection surfaces can focus the light while directing it straight forwards afterwards, due to refraction. In order to keep the refracted beam parallel to the incident beam the relation between the refractive index n and the opening angle γ between the centrally located total internal reflection surfaces are given as:

$$n = \frac{\cos\left(\frac{1}{2}\gamma\right)}{\cos\left(\frac{3}{2}\gamma\right)} \tag{1}$$

This expression is an approximation, as the total internal reflection surfaces are not flat but convex. Additionally, the angle of incidence also depends somewhat on the opposing cylinder lens. This relation sets an upper limit on the opening angle at 60°, and it is found that this requirement also ensures that the first reflection is always a total internal reflection (assuming light beams along the optical axis). As an example, for a refractive index of 3.8, an approximate opening angle of 51° is found.

As with all Fresnel zone based devices, this unit has a significant diffraction pattern, and is therefore not well suited for coherently illuminated scenes.

3. EXPERIMENTS

The experiments presented here were originally reported earlier[8]. The setup used is conceptually that of Figure 2. An image of the experimental camera is shown in Figure 4. The linear array is actually an uncooled 2-D PbSe imager, sensitive in the 1.8-5.0 µm spectral range. The 32×32 pixel imager from New Infrared Technologies operated at 100 Hz frame rate. The detector array was operating as a linear array through software binning. This enabled observing the raw imaging data together with the reconstruction data. The circular aperture was emulated through the selection of active pixels during binning. A setup was made to display several steps of the processing, including the recorded raw data, the result of the binning process, filtering of the linear scan, back projection of the last scan and the reconstructed image. The camera was operating at a fixed 100 Hz frame rate, and the scan speed was adjusted to the number of desired angular scans, using a simple tracker of the number of frames being recorded. This was achieved using a stepper motor (Smart Motor from Moog Animatics)

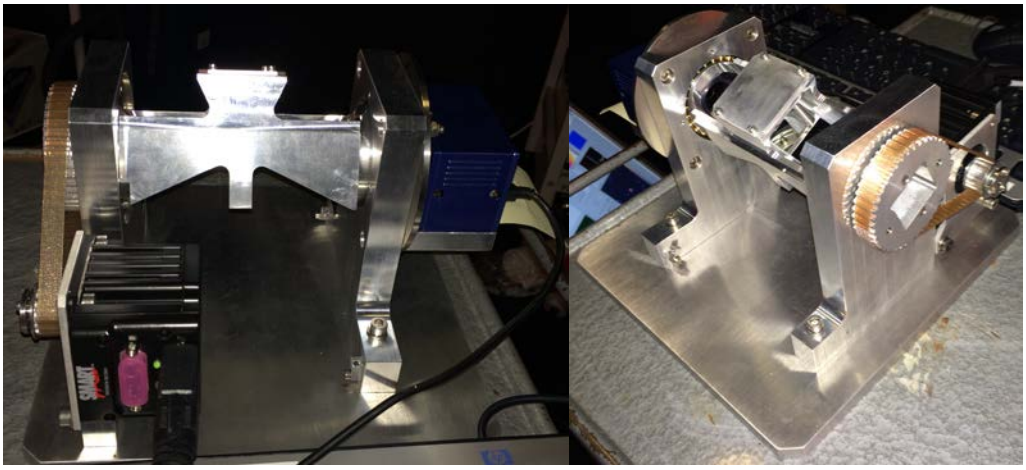

Figure 4. Experimental spin scan TOSCA imager. The detector array (blue box) is an uncooled 32×32 pixel mid wave infrared detector array, from New Infrared Technologies. The 2-D imager was converted to a linear array through binning. A Moog Animatics Smart Motor was used to drive the scanner. The scanner itself, consisting of three plane mirrors mounted together as a rotating unit, are held between the two vertical brackets.

Figure 5. Halloween mask without (left) and with (middle) a Germanium substrate on the nose. The mask was put in front of a black body (right) operated at 300°C. The mask was cooled down to room temperature using a regular fan.

The imager was observing several targets: a single pinhole and double pinhole, and a Halloween mask targets, shown in Figure 5. To get a measure of the dynamics in the system, one of the pinholes and the nose of the Halloween mask were covered by a 2 mm thick uncoated Ge substrate during some experiments. The Ge substrate was found to reduce the signal from the blackbody by an order of magnitude, compared to the mask background. Due to detector drift, a 1 point non-uniformity correction was applied to the camera prior to each recording.

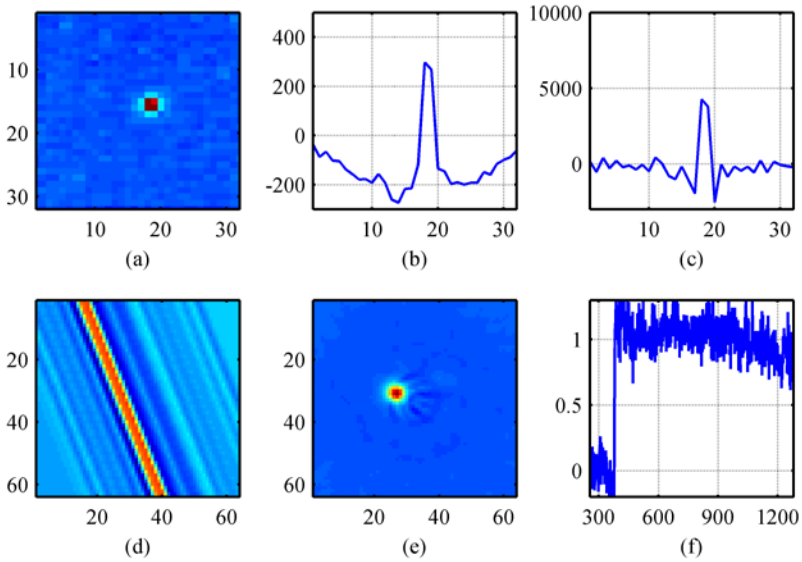

Figure 6. Single point target, back illuminated by the 300°C black body. (a) Raw image from the detector. (b) Single scan from one angular orientation (corresponding to one camera frame. (c) Filtered single scan. (d) Back projection of the current filtered scan. 99 such back projections (one for each scan angle) are added together to form the final reconstruction (e). (f) Energy monitoring of each scan as a function of time.

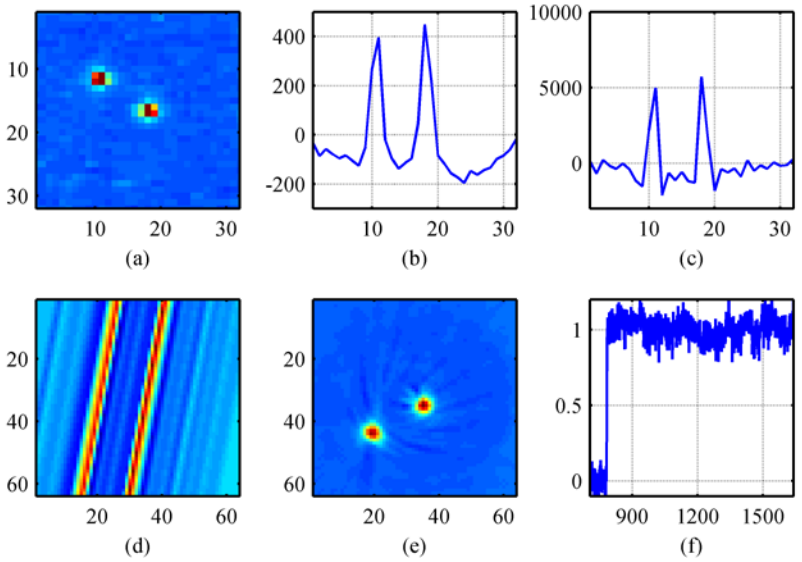

Figure 7. Double point target, back illuminated by the 300°C black body. (a) Raw image from the detector. (b) Single scan from one angular orientation (corresponding to one camera frame. (c) Filtered single scan. (d) Back projection of the current filtered scan. 99 such back projections (one for each scan angle) are added together to form the final reconstruction (e). (f) Energy monitoring of each scan as a function of time.

As can be seen in Figure 6-8, some errors are visible when hot spots appear in the field of view. Even if the patterns associated to the location were significant, the weak signal from the optically filtered source was still visible in the reconstructed image.

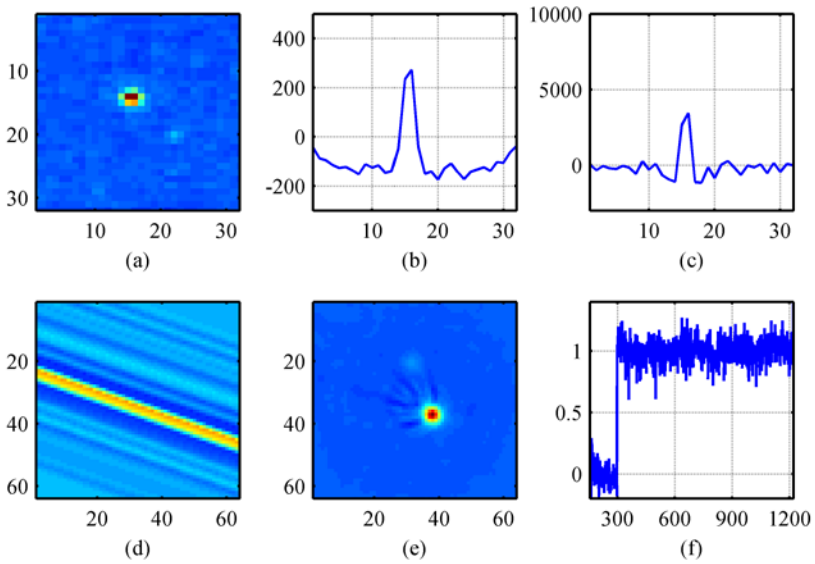

Figure 8. Double point target, back illuminated by the 300°C black body, with one pinhole covered by the Ge substrate. (a) Raw image from the detector. (b) Single scan from one angular orientation (corresponding to one camera frame. (c) Filtered single scan. (d) Back projection of the current filtered scan. 99 such back projections (one for each scan angle) are added together to form the final reconstruction (e). (f) Energy monitoring of each scan as a function of time.

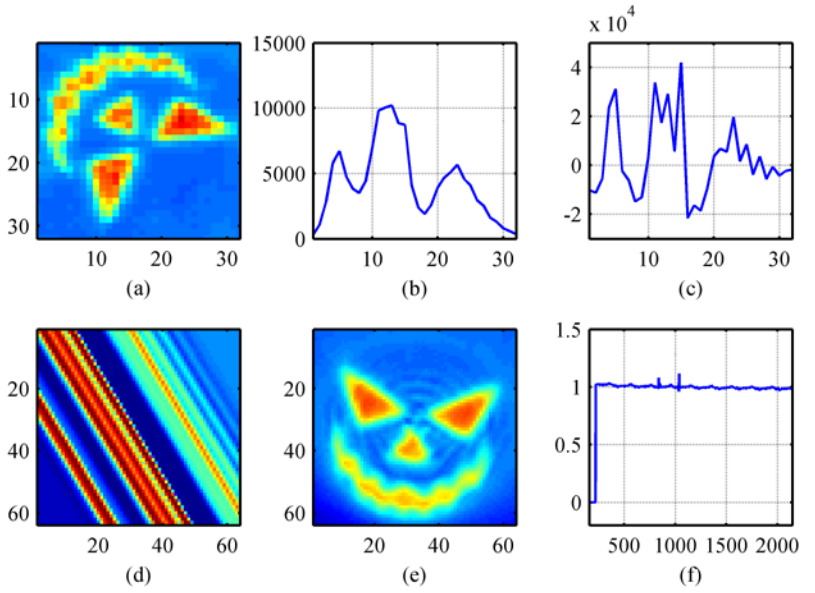

Figure 9. Halloween mask target, backlit by the 300°C black body. (a) Raw image from the detector. (b) Single scan from one angular orientation (corresponding to one camera frame. (c) Filtered single scan. (d) Back projection of the current filtered scan. 99 such back projections (one for each scan angle) are added together to form the final reconstruction (e). (f) Energy monitoring of each scan as a function of time.

Figures 9-10 shows the reconstruction of the Halloween mask with or without the Ge substrate covering the nose. It can here be seen that the nose is no longer visible when its signature is small. This is due to the significant interference fringe pattern, caused by the complex scene.

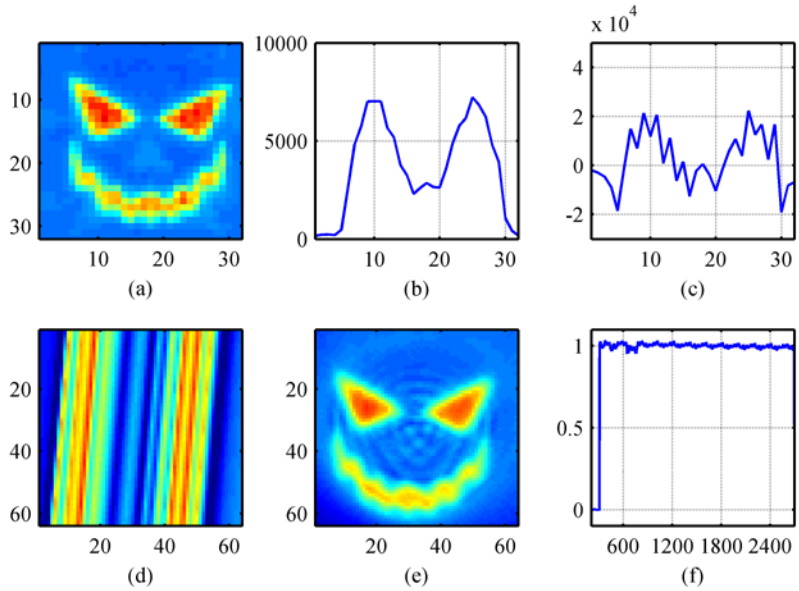

Figure 10. Halloween mask target, backlit by the 300°C black body, and with the Ge substrate covering the nose. (a) Raw image from the detector. (b) Single scan from one angular orientation (corresponding to one camera frame. (c) Filtered single scan. (d) Back projection of the current filtered scan. 99 such back projections (one for each scan angle) are added together to form the final reconstruction (e). (f) Energy monitoring of each scan as a function of time.

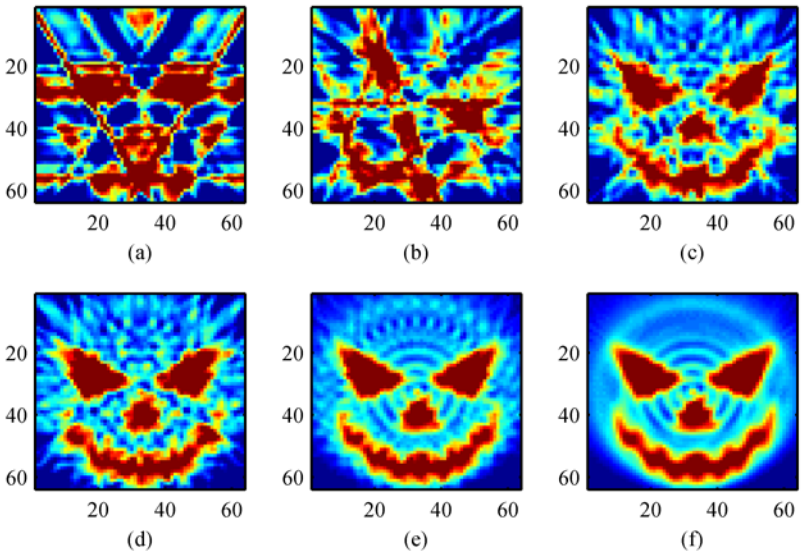

Figure 11. Halloween mask target, backlit by the 300°C black body, reconstructed using the regular (linear) reconstruction technique with (a) 3 scans, (b) 5 scans, (c) 9 scans, (d) 11 scans, (e) 33 scans, and (f) 99 scans.

Figure 11 gives an impression of how many scan angles are required to extract imaging information. As can be seen, at 3 angles it is almost impossible to recognize anything in the image. It may still be possible to remove some of the noise in the image, for example by using nonlinear techniques, but it appears clear that more information is required. Already at around 10 angular scans it appears, though, that the main features in the image are visible. It isn't until the number of scans equals the number of pixels around the perimeter, that features relating to a limited number of angular scans cease to represent discernible in the image, though. It has been found that the remaining features in Figure 11(f) are due to non-uniformities in detector gain and/or offset.

4. CONCLUSIONS

A new class of imagers has been discovered, called the spin scan TOSCA imager. Compared to the previous conical scan TOSCA imager, this type of imager provides an order of magnitude better signal-to-noise ratio, requires lower bandwidth and is simpler to build. In addition, the potential 100% coverage of the field of view enables monitoring and characterization of high speed transient processes, even much higher than the frame rate. A new compact compound lens, consisting of a cylinder lens and a Fresnel reflector has been described, to the author's knowledge for the first time. Experimental work is presented on a spin scan array-based TOSCA imager operating in the mid-wave infrared spectral region (1.8-5.0 μm).

REFERENCES

[1] Hovland, H., "Tomographic scanning imaging seeker," Proc. SPIE 5430, 76-85 (2004).
[2] Hovland, H., "Specialized tomographic scanning imaging seeker," Proc. SPIE 5778, 725-738 (2005).
[3] Hovland, H., "Optimization of the tomographic scanning (TOSCA) imager," Proc. SPIE 6569, 65690I (2007).
[4] Hovland, H., "Construction and demonstration of a multispectral tomographic scanning imager (TOSCA)," Opt. Express 21(4), 4688-4702 (2013).
[5] Hovland, H., "Experimental tomographic scanning (TOSCA) imagers," Proc. SPIE 9070, 65690I90700H (2014).
[6] Kak, A., Slaney, M., [Principles of computerized tomographic imaging], IEEE Press, New York, 70-71 (1988).
[7] Hovland, H., "Tomographic scanning imager," Opt. Express 17(14), 11371-11387 (2009).
[8] Hovland, H., "Spin scan tomographic array-based imager," Opt. Express 22(26), 31999-32015 (2014).
[9] Schmidt, W. H. K., "A proposed X-ray focusing device with wide field of view for use in X-ray astronomy," Nucl. Instr. And Methods 127, 285-292 (1975).
[10] Angel, J. R. P., "Lobster eyes as X-ray telescopes," Astrophys. J. 233, 364-373 (1979).